https://www.scientificarchives.com/journal/journal-of-nanotechnology-and-nanomaterials

Journal of Nanotechnology and Nanomaterials Review Article

Current Progress in Vanadium Oxide Nanostructures and Its Composites as Supercapacitor Electrodes

Raktima Basu*, Sandip Dhara*

Surface and Nanoscience Division, Indira Gandhi Centre for Atomic Research, Homi Bhabha National Institute, Kalpakkam-603102, India

*Correspondence should be addressed to Raktima Basu; raktimabasu14@gmail.com, S. Dhara; dhara@igcar.gov.in

Received date: August 27, 2020, **Accepted date:** October 12, 2020

Abstract

In recent years, vanadium oxides have gained immense attention in the field of energy storage devices due to their low-cost, layered structure and multi-valency despite their limited electrical conductivity and lower structural stability. In this brief review, we have focused on electrochemical properties of the stoichiometric vanadium oxides along with VO_x composites. The morphology engineering, doping with heteroatom and formation of composites with carbon-based materials and/or conducting polymers in enhancing the supercapacitive performances of the vanadium oxides are discussed in detail. Finally, the potentiality and challenges of vanadium oxides nanocomposites for supercapacitor applications are discussed.

Keywords: Supercapacitor, Vanadium oxide, Specific capacitance, Pseudocapacitance, Phase transition

Introduction

In recent time, supercapacitors (SCs) are one of the emerging technologies used for clean energy prospect. The higher power density, low specific energy, longer cycle life, and environmental affability made the SCs superior compared to conventional batteries. However, the scientific community is working towards increasing the specific energy of SCs by finding a suitable electrode material. Carbon materials, conducting polymers, and metal oxide or hydroxides are reported to be suitable candidates as electrodes for SC [1-3]. Carbon materials such as activated carbon, carbon nanotube and graphene provide excellent electrical conductivity and chemical stability [4], however, they come with narrow charge storage capacity and relatively low energy density [1]. On the other hand, the conducting polymers are a good choice as a pseudocapacitor [3]. Nevertheless, the electrochemical stability of conducting polymer is poor. Towards this end, transition metal oxides (TMOs) are alternative candidates due to their multiple oxidation states and rapid redox kinetics [2,5-7]. Amongst other TMOs [8-10], vanadium oxides have received recent attention owing to their low-cost, variety of valence states, and abundant sources [11-13]. V is a transition metal ([Ar]$3d^3 4s^2$) with valences in the range of +2 to +5 with major oxides as VO, V_2O_3, VO_2, and V_2O_5 [14]. However, the V-O phase diagram comprises mixed-valence oxides comprehending two oxidation states, e.g. V_4O_9, V_6O_{13}, V_8O_{15}, V_7O_{13}, V_6O_{11}, among others which permit conversion between oxides of different stoichiometry easily and make it unstable during charging-discharging cycle. As the composition, oxidization state, and structural phase of a material have a significant role on electrochemical properties; the exchange of valency along with structural instability for these materials result in poor electrochemical and cycle performance. Issues related to the presence of multiple valence states of V [13], as well as its stability affecting retention of capacitance and its efficiency, are found to hinder further utility in SCs. The poor charge storage properties and electrical conductivity of vanadium oxides are reported to be succeeded by fabricating directly on the current collector, doping element, or by nanostructure engineering. There are several reports on SC properties of VO_x composites as well as individual vanadium oxides such as VO_2, V_2O_3, and V_2O_5 [3,15-26]. In this context, this mini review presents a summary of recent developments in vanadium oxide based supercapacitor along with future developments, prospects, and challenges.

Electrochemical Properties of Vanadium Dioxide

Vanadium dioxide (VO_2) is known to be stabilized in different polymorphs, including VO_2(A), VO_2(B), VO_2(C), VO_2(D), among others. [27]. Among the VO_2 polymorphs, VO_2(B) attracts much attention for its well known MIT at a technologically important temperature of 340K, which is very close to room temperature [28]. VO_2(B) crystallizes in rutile tetragonal (R; space group $P4_2/mnm$) and monoclinic (M1; space group $P2_1/c$) structure above and below the transition temperature, respectively [29,30]. In the high-temperature R phase, V atoms are equally spaced, forming linear chains along the c_R axis with each V atom surrounded by an oxygen octahedron [31]. The lattice parameters are c_R = 2.85 Å, and a_R =b_R = 4.55 Å. Whereas in low-temperature monoclinic phase, the volume of the unit cell becomes double than that of R phase with lattice parameters a_{M1} = 5.70 Å, b_{M1} = 4.55 Å, c_{M1} = 5.38 Å, and β_{M1} = 123° [32]. The approximate crystallographic relationship between M1 and R phase is $a_{M1} \leftrightarrow 2c_R$, $b_{M1} \leftrightarrow a_R$, and $c_{M1} \leftrightarrow b_R$- c_R [33]. In the M1 phase, there are significant differences in the arrangement of V along c_R axis. The V atoms form pair, and the pairs tilt along the c_R axis making the surrounding octahedron deformed. Besides M1, two more metastable phases of monoclinic M2 having space group $C2/m$ and triclinic T (alternatively monoclinic M3) with space group $C\bar{1}$ are also reported in the process of the phase transition from M1 to R [34].

There are several reports on the supercapacitive performance of VO_2(B) in the M1 phase. However, its low rate capability and cycling instability become obstacles to serve as a commercial supercapacitor. The modification in structure designing has been adopted to overcome the barrier. Zhang et al. [35] prepared template-free 3D hollow spherical cages (shown in figures 1a-b) by hydrothermal method, which showed a specific capacitance of 1175 mF·cm^{-2} (336 F·g^{-1}) with adequate stability, and 68% of the capacitance was retained after 10,000 cycles.However, 2D nanosheet of VO_2 is reported to be a more eligible candidate for electrochemical performance than that of its 3D counterpart because of large specific surface area shortening the diffusion path of ion and thereby enhancing the redox reaction. Ndiaye et al. [36] obtained specific capacitance of 663 F·g^{-1} at the scan rate of 5 mV·s^{-1} and excellent cycling stability after 5000 cycles at the current density of 10 A·g^{-1} for VO_2 nanosheets. The 2D nanosheets (Figures 1c and 1d), while assembled with the structure of carbonized iron-polyaniline (C-FP), exhibited a specific capacity of 47 mAh·g^{-1} at a current density of 1 A·g^{-1} [37]. In 2D nanosheets, a large specific surface area diminishes the path length of the ion diffusion enabling the execution of the redox reaction effectively. Rakhi et al. [38] reported a specific capacitance of ~ 405 F·g^{-1} at the current density of 1 A·g^{-1} for VO_2 nanosheets in an organic gel electrolyte (1 M $LiClO_4$ in propylene carbonate) with nearly 82% capacitance retention.

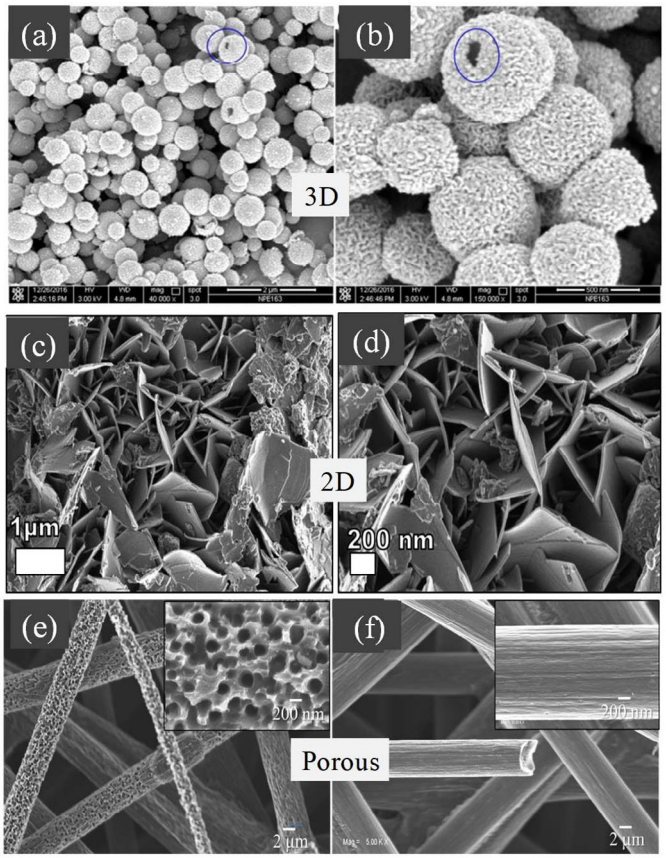

Figure 1: Scanning electron micrograph of **(a-b)** VO_2 3D hollow spherical cages and its higher magnification image; marked circles show broken area [Reprinted with permission from Ref. 36, Copyright 2018 @ Royal Society of Chemistry] **(c-d)** 2D VO_2 nanosheet and its zoomed image [Reprinted with permission of authors from Ref. 37, Copyright 2019 @ American Institute of Physics], **(e)** VO_2 nanoporous structure grown on carbon paper, (f) bare C fiber [Reprinted with permission of authors from Ref. 40, Copyright 2019 @ Nature Publishing Group].

The thin layer of 1D VO_2 nanorods on indium tin oxide - coated glass substrates are also reported [39] to produce a specific capacitance of ~486 mF·cm^{-2} at the scan rate of 10 mV·s^{-1}. Nie et al. [22] reported VO_2@Polyaniline coaxial nanobelts exhibiting a higher specific capacitance of 246 F·g^{-1} at 0.5 A g^{-1} than that of VO_2 nanobelts (160.9 F·g^{-1}). The specific capacitance was almost constant at around 118 mF·cm^{-2} after 5000 cycles at the scan rate of 100 mV·s^{-1}. VO_2 nanoporous structures on carbon fiber in the M1 phase (Figures 1e and 1f) exhibit a specific capacitance of 20.7 mF·cm^{-2} at the current density of 0.3 mA·cm^{-2} [40].

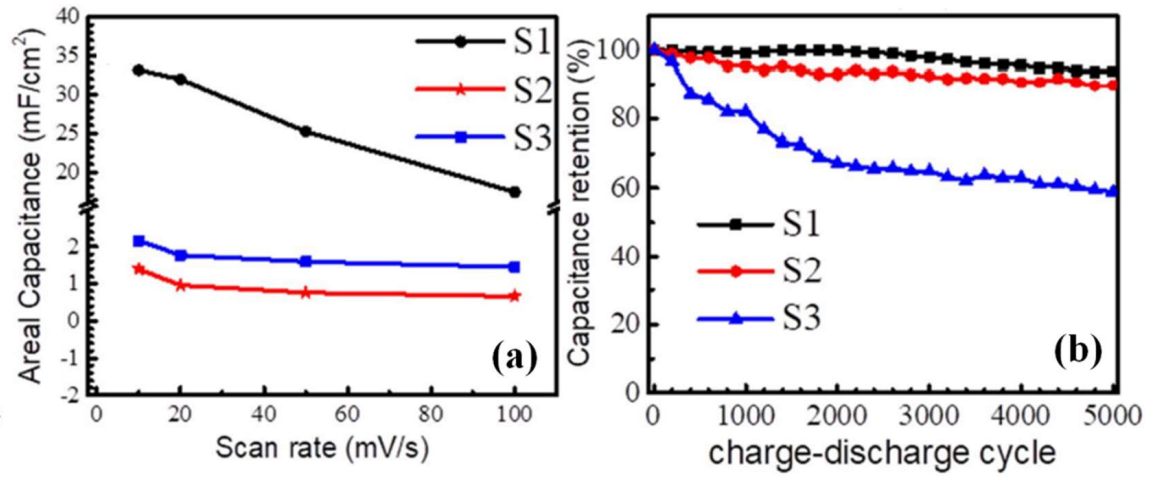

Figure 2: (a) Areal capacitance versus scan rate and **(b)** capacitance retention with charge-discharge cycle of pure M1 (S1), and mixed phases of VO_2 (S2 and S3) [Reprinted with permission of authors from Ref. 40, Copyright 2019 @ Nature Publishing Group].

It also demonstrates capacitance retention of 93.7% and coulombic efficiency of 98.2% for 5000 charge-discharge cycles. However, the similar nanoporous structures in M2 and T phases of VO_2 show poor specific capacitance (Figure 2a) as well as cyclic stability (Figure 2b) because of mixed valency [40].

Another way to enhance the electrochemical performance of VO_2 is by combining with carbon materials, which improve the electrical conductivity. VO_2 nanoflowers on 3D graphene (3DG) networks were reported to exhibit a large specific capacitance of 466 $mF{\cdot}cm^{-2}$, capacitance retention of 63.5% after 3000 cycles by Wang et al. [41]. Ren et al. [42] synthesized VO_2 nanoparticles on edge-oriented graphene foam (EOGF) which exhibit a capacitance of 119 $mF{\cdot}cm^{-2}$ at the scan rate of 2 $mV{\cdot}s^{-1}$. The VO_2(B)/carbon core-shell composites prepared by Zhang et al. [43] exhibited a specific capacitance of 203 $F{\cdot}g^{-1}$ at the current density of 0.2 $A{\cdot}g^{-1}$. Lv et al. [44] prepared VO_2(B) nanobelts/rGO composites with a porous framework, which showed an excellent power density of 7152 $W{\cdot}kg^{-1}$ at the energy density of 3.13 $Wh{\cdot}kg^{-1}$. Shao et al. [23] reported VO_2 demonstrating superior properties as supercapacitor compared to that for the V_2O_5, which was well known for its SC performance. It is due to higher electronic conductivity in VO_2, as compared to V_2O_5, originating from a mixed-valence and structural stability because of the increased edge sharing and the consequent resistance to lattice shearing during cycling [45]. The comparison of various VO_2 based supercapacitors and their synthesis procedures are shown in Table 1.

Nanostructures (Growth Technique)	**Electrolyte**	**Specific Capacitance**	**Current density**	**Cycling stability (%)**	**Ref.**
VO_2 (B) hollow spheres (Solvothermal)	1 M Na_2SO_4/ critical micelle concentration	336 $F{\cdot}g^{-1}$	2 $mA{\cdot}cm^{-2}$	68% (10000 cycles)	[36]
VO_2 nanosheets (Solvothermal)	6 M KOH	663 $F{\cdot}g^{-1}$	10 $A{\cdot}g^{-1}$	99.4% (9000 cycles)	[37]
VO_2 nanosheets (Solvothermal)	6 M KOH	47 $mAh{\cdot}g^{-1}$	1 $A{\cdot}g^{-1}$	89% (10 000 cycles)	[37]
VO_2 nanosheet (Solution Reduction of hydrothermally exfoliated bulk V_2O_5)	1 M $LiClO_4$/PPC	405 $F{\cdot}g^{-1}$	1 $A{\cdot}g^{-1}$	82% (6000 cycles)	[38]

VO_2 nanorod thin films (RF magnetron sputtering)	0.1 M NaOH	486 mF·cm^{-2}	10 mV·s^{-1}	100% (5000 cycles)	[39]
VO_2@Polyaniline coaxial nanobelts (Reactive templated organic layer on solvothermally grown VO_2nanobelt)	0.5 M Na_2SO_4	246 F. g^{-1}	0.5 A. g^{-1}	(28.6%) (1000 cycles)	[22]
Nanoporous VO_2 (Vapour transport of bulk V_2O_5 on C-paper)	Na_2SO_4	20.7 mF·cm^{-2}	0.3 mA·cm^{-2}	93.7% (5000 cycles)	[40]
VO_2 NFs@3DG (Hydrothermally grown VO_2 on 3DG)	0.5 M K_2SO_4	507 F·g^{-1}	3 mA·cm^{-2}	63.5% (3000 cycles)	[41]
VO_2 nanoparticle/EOGF (Hydrothermally grown VO_2 on EOGF)	5 M LiCl	119 mF·cm^{-2}	2 mV·s^{-1}	70% (1500 cycles)	[42]
VO_2(B)/C core-shell (Single pot hydrothermal)	1 M Na_2SO_4	203 F·g^{-1}	0.2 A·g^{-1}	10.4% (100 cycles)	[43]
VO_2(B) nanobelts/rGO (Hydrothermally grown VO_2 on rGO)	0.5 M K_2SO_4	353 F·g^{-1}	1 A·g^{-1}	78% (10 000 cycles)	[44]

Table1: Comparison of various VO_2 based supercapacitors.

Electrochemical Properties of Vanadium Trioxide

Vanadium trioxide (V_2O_3) revels a rhombohedral corundum structure at room temperature, (space group $R\bar{3}c$) [46], where the V atoms pair along the crystal *c*-axis and form honeycomb lattices in the *ab*-plane. Whereas, below the temperature ~150 K, a paramagnetic metallic to an antiferro-magnetic insulating transition happens along with the structural transition to the monoclinic phase (space group I_2/a) [47].

There are very few reports on the electrochemical studies on V_2O_3, mostly because of the poor stability of this material. A binder-free electrode of V_2O_3 nanoflakes on N-doped rGO (Figure 3a) was reported to have an areal capacitance of 216 mF·cm^{-2} at a current density of 1 mA·cm^{-2} (Figure 3b). It also exhibits cycling stability with retention of ~81% of the initial capacitance value after 10,000 cycles (Figure 3c) [48].

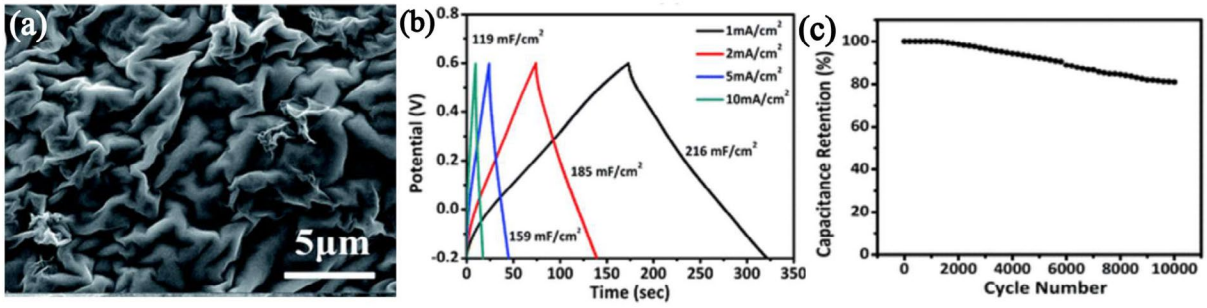

Figure 3: (a) Scanning electron micrograph of the V_2O_3/N-rGO samples, **(b)** The galvanostatic charge-discharge (GCD) curves obtained for the self-supported V_2O_3/N-rGO film electrodes at different current densities. (c) Cycling stability for 10000 cycles [Reprinted with permission from Ref. 48, Copyright 2017 @ Royal Society of Chemistry].

Nanostructures (Growth Technique)	**Electrolyte**	**Specific Capacitance**	**Current density**	**Cycling stability (%)**	**Ref.**
V_2O_3/N-rGO nanoflakes (500 °C NH_3 reduction of V_2O_5 gel/ GO films)	1 M Na_2SO_4	216 mF·cm^{-2}	1 mA·cm^{-2}	81% (10000 cycles)	[48]
V_2O_3/C nanocomposites (Calcination of hydrothermally grown $(NH_4)_2V_3O_8$)	5 M LiCl	458.6 F·g^{-1}	0.5 A·g^{-1}	86% (1000 cycles)	[49]
V_2O_3@C core-shell nanorods (Single pot hydrothermal process using V_2O_5 nanorod)	5 M LiCl	228 F·g^{-1}	0.5 A·g^{-1}	86% (1000 cycles)	[50]
V_2O_3 nanofoam@activated carbon (Calcination of NH_4VO_3 solution and activated C)	1 M $NaNO_3$	185 F·g^{-1}	0.05 A·g^{-1}	49% (100 cycles)	[51]

Table 2: Comparison of various V_2O_3 based supercapacitors.

However, V_2O_3 combined with carbon composites are reported to serve as superior electrode material. Zheng et al. reported V_2O_3/C composites exhibiting high pseudocapacitance of 458.6 F·g^{-1} at 0.5 A·g^{-1}. The composite also shows a retention rate of 86% after 1000 cyclesin aqueous electrolyte [49]. Hu et al. [50] synthesized V_2O_3@C core-shell nanorods with porous structures which exhibited 228, 221, 207, 158, and 127 F·g^{-1} specific capacitances at current densities of 0.5, 1, 2, 5, and 10 A·g^{-1}, respectively. Zhang et al. [51] reported a V_2O_3 nanofoam@ activated carbon composite, which showed a specific capacitance of 185 F·g^{-1} at 0.05 A·g^{-1}. The comparison of various V_2O_3 based supercapacitors fabricated following different process steps, are shown in Table 2.

Electrochemical Properties of Vanadium Pentoxide

Vanadium pentoxide (V_2O_5) stabilizes in various phases including α-V_2O_5, β-V_2O_5, δ-V_2O_5, γ′-V_2O_5, ζ-V_2O_5, and ε′-V_2O_5 [52]. The most well-known phase is α-V_2O_5, which crystallizes into an orthorhombic structure composed of weakly Van der Walls bonded layers of VO_5 pyramids sharing their vertices and corners [53,54]. The unit-cell parameters are a = 11.51 Å, b = 3.56 Å, and c = 4.37 Å [53]. It has space group P_{mmn}, (D_{2h}^{13}) with distorted square-pyramidal coordination symmetry around each V atom. There are three non-equivalent oxygen atoms in each unit cell (denoted as O_I, O_{II}, and O_{III}). O_I is the terminal (vanadyl) oxygen with two different bond lengths. One of them is a strong and short V-O_I bond with a length of 1.577 Å (d_1). Another one is large and weak Van der Waals type connecting two adjacent layers in the V_2O_5 structure, with a bond length of 2.793 Å. Both of these O_I atoms orient almost along the *c*-axis. The two-fold coordinated bridging oxygen (O_{II}) connects two adjacent V atoms with V-O_{II} bond length of 1.78 Å (d_2). The ladder-shaped O_{III} atoms are the three-fold coordinated oxygen with three different V-O_{III} bond lengths of 1.88 (d_3), 1.88 (d_3), and 2.02 Å (d_4) [53].

The SC properties in V_2O_5 is reported to be superior to other vanadium oxides because of its stability and layered structure [19,21-23]. Yang et al. [55] prepared hollow V_2O_5 spheres which showed an excellent capacitance of 479 F·g^{-1} at 5 mV·s^{-1}. V_2O_5 nanofibers showed specific capacitance of 190 F·g^{-1} in aqueous electrolyte (KCl) and 250 F·g^{-1} in the organic electrolyte ($LiClO_4$ in PPC) as reported by Wee et al. [56]. Apart from supercapacitor performance, the change in electrolytes in case of V_2O_5 also controls its mechanical stability and chemical dissolution. Pandit et al. [57] synthesized V_2O_5 thin film on a pliable stainless steel substrate which was reported to exhibit a high specific capacitance of 735 F·g^{-1} at 1 mV·s^{-1} with capacitors retention of 71% after 1000 cycles.

The rGO/V_2O_5 composites showed specific capacitance of 386, 338, 294, 241, and 197 F·g^{-1} at current density of 0.1, 0.2, 0.5, 1, and 2 A·g^{-1}, respectively, as reported by Liu et al. [58]. However, 2D heterostructures of V_2O_5 nanosheets growing on rGO flakes showed relatively high specific capacitance of 653 F·g^{-1} at 1 A·g^{-1} and cyclic stability of 94% after 3000 cycles [59]. Choudhury et al. [60] prepared V_2O_5 nanofiber (VNF)/exfoliated graphene nanohybrid with the mass ratio of 1:0.25 and 1:0.5 with a superior capacitance value of 218 F·g^{-1} at 1 A·g^{-1} for 1:0.5 mass ratio. Balasubramanian et al. [61] reported flowery V_2O_5 structures coated with carbon showing specific

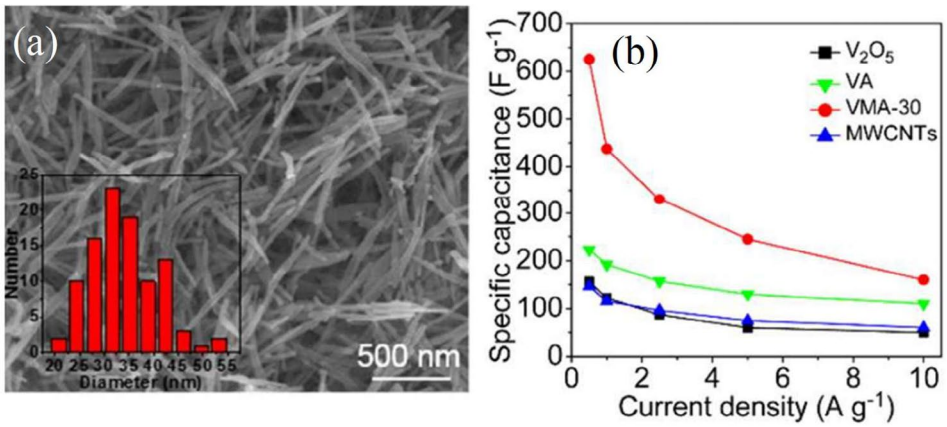

Figure 4: (a) Scanning electron micrograph of V_2O_5 aerogel and diameter distribution of V_2O_5 nanofibers (inset) **(b)** Specific capacitance as a function of current density for raw V_2O_5 powder, MWCNTs, V_2O_5 aerogel and hybrid aerogel of V_2O_3/C nanocomposites (VMA-30) [Reprinted with permission from Ref. 63, Copyright 2015 @ Royal Society of Chemistry].

capacitance of 417 F·g^{-1} at a current density of 0.5 A·g^{-1}. Chen et al. [62] synthesized V_2O_5 nanocomposites with carbon nanotubes (CNT) which provided a capacity of 228 C·g^{-1} between 1.8 and 4.0 V. Wu et al. [63] reported V_2O_5/ multi-walled CNT core/shell hybrid aerogel (Figure 4a), which demonstrated the maximum specific capacitance of 625 F·g^{-1} with outstanding cycle performance (>20000 cycles). The hybrid aerogel showed better performance than that of raw V_2O_5 powder, MWCNTs, and V_2O_5 aerogel (Figure 4b).

However, the insertion of nitrogen atoms into the carbon network enhances the electrochemical performance by restraining the hydrophobicity. Sun et al. [64] reported self-assembled 3D N-carbon nanofibers (CNFs)/V_2O_5 aerogels showing the specific capacitance of 575.6 F·g^{-1} even after 12,000 cycles (97% of the initial value). V_2O_5 also have been combined with conducting polymers *e.g.*, polypyrrole (PPy), poly (3, 4-ethylenedioxythiophene) (PEDOT), and polyaniline (PANI), to enhance the electrical conductivity and prevent the V from dissolving. Qian et al. [65] reported 3D V_2O_5/PPy nanostructures, which exhibited a high specific capacitance of 448 F·g^{-1}. However, Bi et al. [66] showed a comparative study with oxygen vacancy (Ö) resulting with the specific capacitance of 614 F·g^{-1} for VÖ-V_2O_5/PEDOT higher than that of 523 F·g^{-1} for VÖ-V_2O_5/PANI and 437 F·g^{-1} for VÖ-V_2O_5/PPy (Figures 5a and 5b).

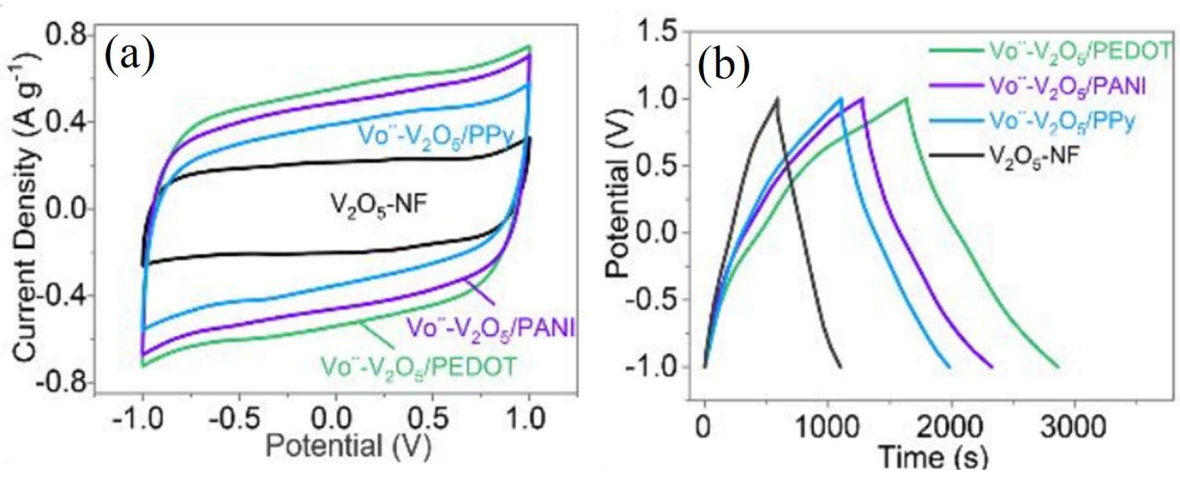

Figure 5: (a) CV curves of V VÖ -V_2O_5/Conducting polymers and V_2O_5-NF at a scan rate of 5 mV. s^{-1}. **(b)** galvanostatic charge-discharge curves of VÖ-V_2O_5/ Conducting polymers and V_2O_5-NF at a current density of 0.5 A. g $^{-1}$[Reprinted with permission from Ref. 66, Copyright 2019 @ Royal Society of Chemistry].

The association of V_2O_5 with other metal oxides is also reported to enhance the electrochemical properties. Xu et al. prepared V_2O_5 nanobelts/TiO_2 nanoflakes composites [67], which exhibited high specific capacitance of 587 $F{\cdot}g^{-1}$ at 0.5 $A{\cdot}g^{-1}$ with good cyclic stability of 97% after 5000 cycles. The V_2O_5-doped α-Fe_2O_3 composites by Nie et al. [68] showed a capacitance value of 150 $F{\cdot}g^{-1}$ over 200 cycles at 6 $A{\cdot}g^{-1}$. CNT-SnO_2-V_2O_5 composites exhibited higher specific capacitance compared to CNT, V_2O_5, and CNT-V_2O_5 [69]. V_2O_5 shows higher performance combined with carbon and other metal oxides than that of the other two phases of vanadium oxides discussed before. The comparison of various V_2O_5 based supercapacitors with involved synthesis techniques are shown in Table 3.

Nanostructures (Growth Technique)	**Electrolyte**	**Specific Capacitance**	**Current density**	**Cycling stability (%)**	**Ref.**
Hollow spherical V_2O_5 (Solvothermal)	5 M $LiNO_3$	479 $F{\cdot}g^{-1}$	5 $mV{\cdot}s^{-1}$	43% (100 cycles)	[55]
V_2O_5 nanofibers (Electrospinning)	(i) 2 M KCl (ii) 1 M $LiClO_4$/PPC	190 $F{\cdot}g^{-1}$ 250 $F{\cdot}g^{-1}$	0.1 $A{\cdot}g^{-1}$		[56]
V_2O_5 complex (Chemical bath deposition)	2 M $LiClO_4$	735 $F{\cdot}g^{-1}$	1 $mV{\cdot}s^{-1}$	71% (1000 cycles)	[57]
rGO/V_2O_5 hybrid aerogel (One-pot Hydrothermally grown)	1 M $LiClO_4$/PPC	384 $F{\cdot}g^{-1}$	0.1 $A{\cdot}g^{-1}$	82.2% (10 000 cycles)	[58]
rGO/V_2O_5nanosheet (Mixing rGO with hydrothermally grown V_2O_5)	1 M KCl	653 $F{\cdot}g^{-1}$	1 $A{\cdot}g^{-1}$	94% (3000 cycles)	[59]
VNF/graphene nanohybrid (Hydrothermally grown VNF mixed with exfoliated graphene)	1 M LiTFSI in acetonitrile	218 $F{\cdot}g^{-1}$	1 $A{\cdot}g^{-1}$	87% (700 cycles)	[60]
Carbon coated flower V_2O_5 (Co-precipitation method followed by annealing at 400 °C)	1 M K_2SO_4	417 $F{\cdot}g^{-1}$	0.5 $A{\cdot}g^{-1}$	100% (2000 cycles)	[61]
CNT/V_2O_5 nanocomposite (One-pot hydrothermal process of V_2O_5 and hydrophilic CNTs)	1 M $LiClO_4$/PPC	228 $C{\cdot}g^{-1}$	20 $mV{\cdot}s^{-1}$	80% (10000 cycles)	[62]
V_2O_5/MWCNT core/shell hybrid aerogels (One-step sol-gel process)	1 M Na_2SO_4	625 $F{\cdot}g^{-1}$	0.5 $A{\cdot}g^{-1}$	120% (20 000 cycles)	[63]
3D N-CNFs/V_2O_5 aerogels (Self-assembly of nanostructured V_2O_5 onto CNF aerogels with N)	1 M Na_2SO_4	595.1 $F{\cdot}g^{-1}$	0.5 $A{\cdot}g^{-1}$	97% (12000 cycles)	[64]
3D V_2O_5/PPy core/shell nanostructures (V_2O_5 by ion exchange attached with PPy)	5 M $LiNO_3$	448 $F{\cdot}g^{-1}$	0.5 $A{\cdot}g^{-1}$	81% (1000 cycles)	[65]
V_2O_5-Conductive polymer nanocables (V_2O_5 sol attached to functionalized polymers)	1 M Na_2SO_4	614 $F{\cdot}g^{-1}$	0.5 $A{\cdot}g^{-1}$	111% (15 000 cycles)	[66]

V_2O_5/TiO_2 composites (Two-step hydrothermal process using Ni foam)	1 M $LiNO_3$	587 $F{\cdot}g^{-1}$	0.5 $A{\cdot}g^{-1}$	92% (1000 cycles)	[67]
V_2O_5-α-Fe_2O_3 composite nanotubes (One-step electrospinning)	3 M KOH	183 $F{\cdot}g^{-1}$	1 $A{\cdot}g^{-1}$	81.5% (200 cycles)	[68]
SnO_2-V_2O_5-CNT (One-pot hydrothermal)	0.1 M KCl	121.39 $F{\cdot}g^{-1}$	100 $mV{\cdot}s^{-1}$	85.8% (100 cycles)	[69]

Table 3: Comparison of various V_2O_5 based supercapacitors.

Large scale production, however, can perhaps be considered for the most stable phase of V_2O_5 with its optimum performance as a supercapacitor. Thus, looking into the economic prospect, materials involving sol-gel route synthesis [63,66,70] and electrospinning [56] may be adopted for the growth of various V_2O_5.

Electrochemical Properties of VOx

Other than the stoichiometric oxides of V, there are also reports for electrochemical applications of multi-valent vanadium oxides (VO_x). The V-O phase diagram comprises mixed-valence oxides comprehending two oxidation states, namely, V_3O_7, V_6O_{13}, V_8O_{15}, V_7O_{13}, V_6O_{11}, among others [71]. It permits conversion between oxides of different stoichiometry. Huang et al. [72] reported a high areal capacitance of 1.31 $F{\cdot}cm^{-2}$ from VO_x functionalized by a carbon nanowire array. V_3O_7 was reported to get converted to V_6O_{13} at the lowest potential of -0.6 V and V_2O_5 at the highest potential of 0.2 V. Zhao et al. [73] prepared NC-coated nest-like V_3O_7 which showed the specific capacity of 660.63 $F{\cdot}g^{-1}$ at 0.5 $A{\cdot}g^{-1}$ (Figure 6a), a significantly higher than that of V_3O_7 (362.63 $F{\cdot}g^{-1}$). NC-V_3O_7 exhibited 80.47% of the initial capacitance at 10 $A{\cdot}g^{-1}$ after 4000 cycles, which is 23.16% higher than that of V_3O_7 (Figure 6b).

V_6O_{13} has stimulated extensive attention owing to its high specific capacitance and decent cycle ability for Li batteries. However, there are very few reports on its SC performance. V_6O_{13} is known as a mixed-valence oxide as it exists between the V^{4+} and V^{5+} oxidation states with 2:1 ratio [74], which increases the electronic conductivity of the material. Zhai et al. [75] reported V_6O_{13} as well as sulfur-doped, oxygen-deficient V_6O_{13-x} as an anode electrode.

V_6O_{13-x} provides a capacitance of 1353 $F{\cdot}g^{-1}$ at a current density of 1.9 $A{\cdot}g^{-1}$ and outstanding capacitance retention of 92.3% after 10,000 cycles. Pang et al. [76] reported the high electrochemical performance of 3D microflower structure of V_4O_9 supercapacitors (~392 $F{\cdot}g^{-1}$).

Conclusion and Outlook

This brief review deals with the electrochemical performances of vanadium oxides and its composites as supercapacitors. Vanadium oxides have attracted

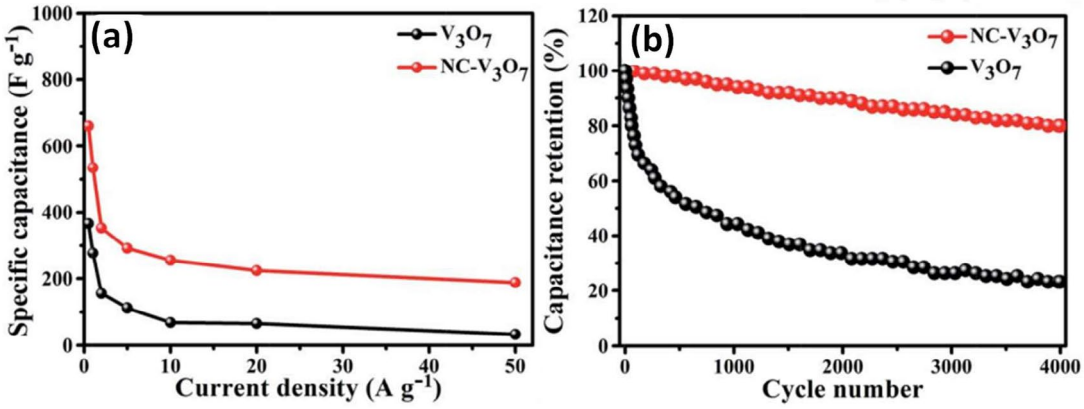

Figure 6: (a) Specific capacitance of V_3O_7 and NC-V_3O_7 as a function of current density and **(b)** cycling performance of V_3O_7 and NC-V_3O_7 at a current density of 10 A g^{-1} [Reprinted with permission from Ref. 73, Copyright 2019 @ Royal Society of Chemistry].

tremendous attention in electrochemistry due to their multi-valency, low cost and abundant sources on earth. However, poor electrical conductivity, structural instability, poor specific capacitance and low energy density limit their practical applications. The scientific community is working towards removing the obstacles by morphology engineering (increase the specific surface area), doping with a heteroatom (reduce hydrophobicity and structural stability), combined with carbon-based materials and/or conducting polymers (increasing conductivity) and so on. The structure designing increases the specific surface area and offer more active sites which in turn increases the contact between the material and electrolyte, generates more redox reactions, and enhances the electrochemical performance of the materials. It has been observed from the previous studies that nanostructures with porosity are the best choice for increasing supercapacitive performance. On the other hand, combining with composites increases the specific capacity, cyclic stability, and finally energy and power density. Comments are also made for the commercial viability in terms of large area synthesis of a stable phase of vanadium oxide with optimized supercapacitance properties. Finding a proper composite material for a specific vanadium oxide is still a challenge for future development. Finally, as vanadium oxides are prone to change the oxidization state, in-situ characterization techniques are likely to be carried out during the electrochemical processes. Most of the vanadium oxides also undergo electrical, magnetic, and/or structural transition with minimal change in the electric field, temperature, or pressure. Therefore, to understand the change in phases and its role in the electrochemical process, advanced in-situ characterization techniques should be incorporated.

References

1. Inagaki M, Konno H, Tanaike O. Carbon materials for electrochemical capacitors. Journal of Power Sources. 2010 Dec 15;195(24):7880-903.

2. Lokhande CD, Dubal DP, Joo OS. Metal oxide thin film based supercapacitors. Current Applied Physics. 2011 May 1;11(3):255-70.

3. Shown I, Ganguly A, Chen LC, Chen KH. Conducting polymer-based flexible supercapacitor. Energy Science & Engineering. 2015 Jan;3(1):2-6.

4. Zhao T, Ji X, Bi P, Jin W, Xiong C, Dang A, et al. In situ synthesis of interlinked three-dimensional graphene foam/polyaniline nanorod supercapacitor. Electrochimica Acta. 2017 Mar 10;230:342-9.

5. Hardani K, Buazar F, Ghanemi K, Kashisaz M, Baghlani-Nezhad MH, Khaledi-Naseb A, et al. Removal of toxic mercury (II) from water via Fe3O4/hydroxyapatite nanoadsorbent: an efficient, economic and rapid approach. AASCIT Journal of Nanoscience. 2015;1(1):11-8.

6. Buazar F, Alipouryan S, Kroushawi F, Hossieni SA. Photodegradation of odorous 2-mercaptobenzoxazole through zinc oxide/hydroxyapatite nanocomposite. Applied Nanoscience. 2015 Aug 1;5(6):719-29.

7. Buazar F, Sweidi S, Badri M, Kroushawi F. Biofabrication of highly pure copper oxide nanoparticles using wheat seed extract and their catalytic activity: A mechanistic approach. Green Processing and Synthesis. 2019 Jan 28;8(1):691-702.

8. Zhou Z, Zhang Q, Sun J, He B, Guo J, Li Q, et al. Metal–organic framework derived spindle-like carbon incorporated α-Fe_2O_3 grown on carbon nanotube fiber as anodes for high-performance wearable asymmetric supercapacitors. ACS Nano. 2018 Sep 7;12(9):9333-41.

9. Zhang Q, Xu W, Sun J, Pan Z, Zhao J, Wang X, et al. Constructing ultrahigh-capacity zinc–nickel–cobalt oxide@ $Ni(OH)_2$ core–shell nanowire arrays for high-performance coaxial fiber-shaped asymmetric supercapacitors. Nano Letters. 2017 Dec 13;17(12):7552-60.

10. Zhang Q, Sun J, Pan Z, Zhang J, Zhao J, Wang X, et al. Stretchable fiber-shaped asymmetric supercapacitors with ultrahigh energy density. Nano Energy. 2017 Sep 1;39:219-28.

11. Yan Y, Li B, Guo W, Pang H, Xue H. Vanadium based materials as electrode materials for high performance supercapacitors. Journal of Power Sources. 2016 Oct 15;329:148-69.

12. Man P, Zhang Q, Sun J, Guo J, Wang X, Zhou Z, et al. Hierarchically structured VO_2@ PPy core-shell nanowire arrays grown on carbon nanotube fibers as advanced cathodes for high-performance wearable asymmetric supercapacitors. Carbon. 2018 Nov 1;139:21-8.

13. Zhang Q, Wang X, Pan Z, Sun J, Zhao J, Zhang J, et al. Wrapping aligned carbon nanotube composite sheets around vanadium nitride nanowire arrays for asymmetric coaxial fiber-shaped supercapacitors with ultrahigh energy density. Nano Letters. 2017 Apr 12;17(4):2719-26.

14. Haber J. Fifty years of my romance with vanadium oxide catalysts. Catalysis Today. 2009 Apr 30;142(3-4):100-13.

15. Ma XJ, Zhang WB, Kong LB, Luo YC, Kang L. VO_2: from negative electrode material to symmetric electrochemical capacitor. RSC Advances. 2015;5(118):97239-47.

16. Hu C, Xu H, Liu X, Zou F, Qie L, Huang Y, et al. VO_2/TiO_2 nanosponges as binder-free electrodes for high-performance supercapacitors. Scientific Reports. 2015 Nov 4;5:16012.

17. Lee M, Wee BH, Hong JD. High performance flexible supercapacitor electrodes composed of ultralarge graphene sheets and vanadium dioxide. Advanced Energy Materials. 2015 Apr;5(7):1401890.

18. Senthilkumar ST, Selvan RK, Ponpandian N, Melo JS, Lee YS. Improved performance of electric double layer capacitor using redox additive (VO^{2+}/VO_2^+) aqueous electrolyte. Journal of Materials Chemistry A. 2013;1(27):7913-9.

19. Huang G, Li C, Sun X, Bai J. Fabrication of vanadium oxide, with different valences of vanadium,-embedded carbon fibers and their electrochemical performance for supercapacitor. New Journal of Chemistry. 2017;41(17):8977-84.

20. Tang K, Li Y, Li Y, Cao H, Zhang Z, Zhang Y, et al. Self-reduced VO/VO_x/carbon nanofiber composite as binder-free electrode for supercapacitors. Electrochimica Acta. 2016 Aug 10;209:709-18.

21. Wang J, Zhang X, Zhang Y, Abas A, Zhao X, Yang Z, et al. Lightweight, interconnected VO_2 nanoflowers hydrothermally grown on 3D graphene networks for wide-voltage-window supercapacitors. RSC Advances. 2017;7(56):35558-64.

22. Nie G, Lu X, Zhu Y, Chi M, Gao M, Chen S, et al. Reactive Template Synthesis of Inorganic/Organic VO_2@ Polyaniline Coaxial Nanobelts for High-Performance Supercapacitors. ChemElectroChem. 2017 May;4(5):1095-100.

23. Shao J, Li X, Qu Q, Zheng H. One-step hydrothermal synthesis of hexangular starfruit-like vanadium oxide for high power aqueous supercapacitors. Journal of Power Sources. 2012 Dec 1;219:253-7.

24. Hu L, Yu L, Zhao C, Long X, Chen W. Synthesis and characterization of VO_2/mesoporous carbon composites for hybrid capacitors. Journal of Wuhan University of Technology-Mater. Sci. Ed.. 2010 Aug 1;25(4):574-8.

25. Li M, Sun G, Yin P, Ruan C, Ai K. Controlling the formation of rodlike V_2O_5 nanocrystals on reduced graphene oxide for high-performance supercapacitors. ACS Applied Materials & Interfaces. 2013 Nov 13;5(21):11462-70.

26. Zhu J, Cao L, Wu Y, Gong Y, Liu Z, Hoster HE, et al. Building 3D structures of vanadium pentoxide nanosheets and application as electrodes in supercapacitors. Nano Letters. 2013 Nov 13;13(11):5408-13.

27. Srivastava A, Rotella H, Saha S, Pal B, Kalon G, Mathew S, et al. Selective growth of single phase VO_2 (A, B, and M) polymorph thin films. APL Materials. 2015 Feb 1;3(2):026101.

28. Morin FJ. Oxides which show a metal-to-insulator transition at the Neel temperature. Physical Review Letters. 1959 Jul 1;3(1):34.

29. Haverkort MW, Hu Z, Tanaka A, Reichelt W, Streltsov SV, Korotin MA, et al. Orbital-assisted metal-insulator transition in VO_2. Physical Review Letters. 2005 Nov 2;95(19):196404.

30. Kim HT, Lee YW, Kim BJ, Chae BG, Yun SJ, Kang KY, et al. Monoclinic and correlated metal phase in VO_2 as evidence of the Mott transition: coherent phonon analysis. Physical Review Letters. 2006 Dec 26;97(26):266401.

31. Zylbersztejn AM, Mott NF. Metal-insulator transition in vanadium dioxide. Physical Review B. 1975 Jun 1;11(11):4383.

32. Marezio M, Dernier PD, Santoro A. Twinning in Cr-doped VO_2. Acta Crystallographica Section A: Crystal Physics, Diffraction, Theoretical and General Crystallography. 1973 Nov 1;29(6):618-21.

33. Goodenough JB. The two components of the crystallographic transition in VO_2. Journal of Solid State Chemistry. 1971 Nov 1;3(4):490-500.

34. Strelcov E, Tselev A, Ivanov I, Budai JD, Zhang J, Tischler JZ, et al. Doping-based stabilization of the M2 phase in free-standing VO_2 nanostructures at room temperature. Nano Letters. 2012 Dec 12;12(12):6198-205.

35. Zhang Y, Jing X, Cheng Y, Hu T, Changgong M. Controlled synthesis of 3D porous VO_2 (B) hierarchical spheres with different interiors for energy storage. Inorganic Chemistry Frontiers. 2018;5(11):2798-810.

36. Ndiaye NM, Masikhwa TM, Ngom BD, Madito MJ, Oyedotun KO, Dangbegnon JK, et al. Effect of growth time on solvothermal synthesis of vanadium dioxide for electrochemical supercapacitor application. Materials Chemistry and Physics. 2018 Aug 1;214:192-200.

37. Ndiaye NM, Madito MJ, Ngom BD, Masikhwa TM, Mirghni AA, Manyala N, et al. High-performance asymmetric supercapacitor based on vanadium dioxide and carbonized iron-polyaniline electrodes. AIP Advances. 2019 May 10;9(5):055309.

38. Rakhi RB, Nagaraju DH, Beaujuge P, Alshareef HN. Supercapacitors based on two dimensional VO_2 nanosheet electrodes in organic gel electrolyte. Electrochimica Acta. 2016 Dec 1;220:601-8.

39. Reddy IN, Sreedhar A, Shim J, Gwag JS. Multifunctional monoclinic VO_2 nanorod thin films for enhanced energy applications: Photoelectrochemical water splitting and supercapacitor. Journal of Electroanalytical Chemistry. 2019 Feb 15;835:40-7.

40. Basu R, Ghosh S, Bera S, Das A, Dhara S. Phase-pure VO_2 nanoporous structure for binder-free supercapacitor performances. Scientific Reports. 2019 Mar 15;9(1):1-1.

41. Wang J, Zhang X, Zhang Y, Abas A, Zhao X, Yang Z, et al. Lightweight, interconnected VO_2 nanoflowers hydrothermally grown on 3D graphene networks for wide-voltage-window supercapacitors. RSC Advances. 2017;7(56):35558-64.

42. Ren G, Zhang R, Fan Z. VO_2 nanoparticles on edge oriented graphene foam for high rate lithium ion batteries and supercapacitors. Applied Surface Science. 2018 May 31;441:466-73.

43. Zhang Y, Zheng J, Hu T, Tian F, Meng C. Synthesis and supercapacitor electrode of VO_2 (B)/C core–shell composites with a pseudocapacitance in aqueous solution. Applied Surface Science. 2016 May 15;371:189-95.

44. Lv W, Yang C, Meng G, Zhao R, Han A, Wang R, et al. VO_2 (B) nanobelts/reduced graphene oxide composites for high-performance flexible all-solid-state supercapacitors. Scientific Reports. 2019 Jul 25;9(1):1-8.

45. Lampe-Önnerud C, Thomas JO, Hardgrave M, Yde-Andersen S. The Performance of Single-Phase V_6O_{13} in the Lithium/Polymer Electrolyte Battery. Journal of the Electrochemical Society. 1995 Nov 1;142(11):3648.

46. Lupi S, Baldassarre L, Mansart B, Perucchi A, Barinov A, Dudin P, et al. A microscopic view on the Mott transition in chromium-doped V_2O_3. Nature communications. 2010 Nov 2;1(1):1-7.

47. Ding Y, Chen CC, Zeng Q, Kim HS, Han MJ, Balasubramanian M, et al. Novel high-pressure monoclinic metallic phase of V_2O_3. Physical Review Letters. 2014 Feb 4;112(5):056401.

48. Hou ZQ, Wang ZY, Yang LX, Yang ZG. Nitrogen-doped reduced graphene oxide intertwined with V_2O_3 nanoflakes as self-supported electrodes for flexible all-solid-state supercapacitors. RSC Advances. 2017;7(41):25732-9.

49. Zheng J, Zhang Y, Meng C, Wang X, Liu C, Bo M, Pei X, Wei Y, Lv T, Cao G. V_2O_3/C nanocomposites with interface defects for enhanced intercalation pseudocapacitance. Electrochimica Acta. 2019 Sep 20;318:635-43.

50. Hu T, Liu Y, Zhang Y, Nie Y, Zheng J, Wang Q, et al. Encapsulating V_2O_3 nanorods into carbon core-shell composites with porous structures and large specific surface area for high performance solid-state supercapacitors. Microporous and Mesoporous Materials. 2018 May 15;262:199-206.

51. Zhang X, Bu Z, Xu R, Xie B, Li HY. V_2O_3 nanofoam@ activated carbon composites as electrode materials of supercapacitors. Functional Materials Letters. 2017 Dec 7;10(06):1750077.

52. Balog P, Orosel D, Cancarevic Z, Schön C, Jansen M. V_2O_5 phase diagram revisited at high pressures and high temperatures. Journal of Alloys and Compounds. 2007 Feb 21;429(1-2):87-98.

53. Enjalbert R, Galy JE. A refinement of the structure of V_2O_5. Acta Crystallographica Section C: Crystal Structure Communications. 1986 Nov 15;42(11):1467-9.

54. Bachmann HG, Ahmed FR, Barnes WH. The crystal structure of vanadium pentoxide. Zeitschrift für Kristallographie-Crystalline Materials. 1961 May 1;115(1-2):110-31.

55. Yang J, Lan T, Liu J, Song Y, Wei M. Supercapacitor electrode of hollow spherical V_2O_5 with a high pseudocapacitance in aqueous solution. Electrochimica Acta. 2013 Aug 30;105:489-95.

56. Wee G, Soh HZ, Cheah YL, Mhaisalkar SG, Srinivasan M. Synthesis and electrochemical properties of electrospun V_2O_5 nanofibers as supercapacitor electrodes. Journal of Materials Chemistry. 2010;20(32):6720-5.

57. Pandit B, Dubal DP, Sankapal BR. Large scale flexible solid state symmetric supercapacitor through inexpensive solution processed V_2O_5 complex surface architecture. Electrochimica Acta. 2017 Jul 10;242:382-9.

58. Liu Z, Zhang H, Yang Q, Chen Y. Graphene/V_2O_5 hybrid electrode for an asymmetric supercapacitor with high energy density in an organic electrolyte. Electrochimica Acta. 2018 Oct 10;287:149-57.

59. Nagaraju DH, Wang Q, Beaujuge P, Alshareef HN. Two-dimensional heterostructures of V_2O_5 and reduced graphene oxide as electrodes for high energy density asymmetric supercapacitors. Journal of Materials Chemistry A. 2014;2(40):17146-52.

60. Choudhury A, Bonso JS, Wunch M, Yang KS, Ferraris JP, Yang DJ, et al. In-situ synthesis of vanadium pentoxide nanofibre/exfoliated graphene nanohybrid and its supercapacitor applications. Journal of Power Sources. 2015 Aug 1;287:283-90.

61. Balasubramanian S, Purushothaman KK. Carbon coated flowery V_2O_5 nanostructure as novel electrode material for high performance supercapacitors. Electrochimica Acta. 2015 Dec 20;186:285-91.

62. Chen Z, Augustyn V, Wen J, Zhang Y, Shen M, Dunn B, et al. High-performance supercapacitors based on intertwined CNT/V_2O_5 nanowire nanocomposites. Advanced Materials. 2011 Feb 8;23(6):791-5.

63. Wu Y, Gao G, Yang H, Bi W, Liang X, Zhang Y, et al. Controlled synthesis of V_2O_5/MWCNT core/shell hybrid aerogels through a mixed growth and self-assembly methodology for supercapacitors with high capacitance and ultralong cycle life. Journal of Materials Chemistry A. 2015;3(30):15692-9.

64. Sun W, Gao G, Zhang K, Liu Y, Wu G. Self-assembled 3D N-CNFs/V_2O_5 aerogels with core/shell nanostructures through vacancies control and seeds growth as an outstanding supercapacitor electrode material. Carbon. 2018 Jun 1;132:667-77.

65. Qian T, Xu N, Zhou J, Yang T, Liu X, Shen X, et al. Interconnected three-dimensional V_2O_5/polypyrrole network nanostructures for high performance solid-state supercapacitors. Journal of Materials Chemistry A. 2015;3(2):488-93.

66. Bi W, Huang J, Wang M, Jahrman EP, Seidler GT, Wang J, et al. V_2O_5–Conductive polymer nanocables with built-in local electric field derived from interfacial oxygen vacancies for high energy density supercapacitors. Journal of Materials Chemistry A. 2019;7(30):17966-73.

67. Xu J, Zheng F, Xi C, Yu Y, Chen L, Yang W, et al. Facile preparation of hierarchical vanadium pentoxide (V_2O_5)/titanium dioxide (TiO_2) heterojunction composite nano-arrays for high performance supercapacitor. Journal of Power Sources. 2018 Nov 15;404:47-55.

68. Nie G, Lu X, Lei J, Jiang Z, Wang C. Electrospun V_2O_5-doped α-Fe_2O_3 composite nanotubes with tunable ferromagnetism for high-performance supercapacitor electrodes. Journal of Materials Chemistry A. 2014;2(37):15495-501.

69. Jayalakshmi M, Rao MM, Venugopal N, Kim KB. Hydrothermal synthesis of SnO_2–V_2O_5 mixed oxide and electrochemical screening of carbon nano-tubes (CNT), V_2O_5, V_2O_5–CNT, and SnO_2–V_2O_5–CNT electrodes for supercapacitor applications. Journal of Power Sources. 2007 Apr 15;166(2):578-83.

70. Kiruthiga R, Nithya C, Karvembu R. Reduced graphene oxide embedded V_2O_5 nanorods and porous honey carbon as high performance electrodes for hybrid sodium-ion supercapacitors. Electrochimica Acta. 2017 Dec 1;256:221-31.

71. Liu K, Lee S, Yang S, Delaire O, Wu J. Recent progresses on physics and applications of vanadium dioxide. Materials Today. 2018 Oct 1;21(8):875-96.

72. Huang ZH, Song Y, Liu XX. Boosting operating voltage of vanadium oxide-based symmetric aqueous supercapacitor to 2 V. Chemical Engineering Journal. 2019 Feb 15;358:1529-38.

73. Zhao D, Zhu Q, Chen D, Li X, Yu Y, Huang X, et al. Nest-like V_3O_7 self-assembled by porous nanowires as an anode supercapacitor material and its performance optimization through bonding with N-doped carbon. Journal of Materials Chemistry A. 2018;6(34):16475-84.

74. Toriyama T, Nakayama T, Konishi T, Ohta Y. Charge and orbital orderings associated with metal-insulator transition in V_6O_{13}. Physical Review B. 2014 Aug 21;90(8):085131.

75. Zhai T, Lu X, Ling Y, Yu M, Wang G, Liu T, et al. A new benchmark capacitance for supercapacitor anodes by mixed-valence sulfur-doped V_6O_{13} – x. Advanced Materials. 2014 Sep;26(33):5869-75.

76. Pang H, Dong Y, Ting SL, Lu J, Li CM, Kim DH, et al. 2D single-or double-layered vanadium oxide nanosheet assembled 3D microflowers: controlled synthesis, growth mechanism, and applications. Nanoscale. 2013;5(17):7790-4.